

# Nanoionics-based resistive switching memories

Many metal–insulator–metal systems show electrically induced resistive switching effects and have therefore been proposed as the basis for future non-volatile memories. They combine the advantages of Flash and DRAM (dynamic random access memories) while avoiding their drawbacks, and they might be highly scalable. Here we propose a coarse-grained classification into primarily thermal, electrical or ion-migration-induced switching mechanisms. The ion-migration effects are coupled to redox processes which cause the change in resistance. They are subdivided into cation-migration cells, based on the electrochemical growth and dissolution of metallic filaments, and anion-migration cells, typically realized with transition metal oxides as the insulator, in which electronically conducting paths of sub-oxides are formed and removed by local redox processes. From this insight, we take a brief look into molecular switching systems. Finally, we discuss chip architecture and scaling issues.

**RAINER WASER<sup>1,2\*</sup> AND MASAKAZU AONO<sup>3,4</sup>**

<sup>1</sup>Institut für Werkstoffe der Elektrotechnik 2, RWTH Aachen University, 52056 Aachen, Germany

<sup>2</sup>Institut für Festkörperforschung/CNI—Center of Nanoelectronics for Information Technology, Forschungszentrum Jülich, 52425 Jülich, Germany

<sup>3</sup>Nanomaterials Laboratories, National Institute for Material Science, 1-1 Namiki, Tsukuba, Ibaraki 305-0044, Japan

<sup>4</sup>ICORP/Japan Science and Technology Agency, 4-1-8 Honcho, Kawaguchi, Saitama 332-0012, Japan

\*e-mail: r.waser@fz-juelich.de

Memory concepts that have been recently pursued range from spin-based memories (magnetoresistive random access memories, or MRAM for short, and related ideas), in which a magnetic field is involved in the resistance switching, to phase-change RAM (PCRAM), in which thermal processes control a phase transition in the switching material from the amorphous to the crystalline state. Yet another class of resistive switching phenomena is based on the electrically stimulated change of the resistance of a metal–insulator–metal (MIM) memory cell, usually called resistance switching RAM, or RRAM for short. The ‘M’ in MIM denotes any reasonably good electron conductor, often different for the two sides, and the ‘T’ stands for an insulator, often ion-conducting material. Typically, an initial electroforming step such as a current-limited electric breakdown is induced in the virgin sample. This step preconditions the system which can subsequently be switched between a conductive ON state and a less conductive OFF state. The necessity of this initial step and its mechanism strongly depend on the switching class, as will be described.

Starting with the report on oxide insulators by Hickmott<sup>1</sup> in 1962, a huge variety of materials in a MIM configuration have been reported to show hysteretic resistance switching. In general, the ‘T’ in MIM can be one of a wide range of binary and multinary oxides and higher chalcogenides as well as organic compounds, and the

‘M’ stands for a similarly large variety of metal electrodes including electron-conducting non-metals. A first period of high research activity up to the mid-1980s has been comprehensively reviewed elsewhere<sup>2–4</sup>. The current period started in the late 1990s, triggered by Asamitsu *et al.*<sup>5</sup>, Kozicki *et al.*<sup>6</sup> and Beck *et al.*<sup>7</sup>.

Before we turn to the basic principles of these switching phenomena, we need to distinguish between two schemes with respect to the electrical polarity required for resistively switching MIM systems. Switching is called unipolar (or symmetric) when the switching procedure does not depend on the polarity of the voltage and current signal. A system in its high-resistance state (OFF) is switched (‘set’) by a threshold voltage into the low-resistance state (ON) as sketched in Fig. 1a. The current is limited by the compliance current of the control circuit. The ‘reset’ into the OFF state takes place at a higher current and a voltage below the set voltage. In this respect, PCRAMs show unipolar switching (without compliance current in this case). In contrast, the characteristic is called bipolar (or antisymmetric) when the set to an ON state occurs at one voltage polarity and the reset to the OFF state on reversed voltage polarity (Fig. 1b). The structure of the system must have some asymmetry, such as different electrode materials or the voltage polarity during the initial electroforming step, in order to show bipolar switching behaviour. In both characteristics, unipolar and bipolar, reading of the state is conducted at small voltages that do not affect the state.

## CLASSIFICATION OF SWITCHING MECHANISMS

In conjunction with the discussion of conceivable switching mechanisms, we must address the question of the geometrical location of the switching event in a MIM structure. With respect to the cross-section of the electrode pad, the switching to the ON state is typically reported as a confined, filamentary effect rather than a homogeneously distributed one, leading to a resistance that is independent of pad size. In planar MIM structures, filaments along the surface are observed

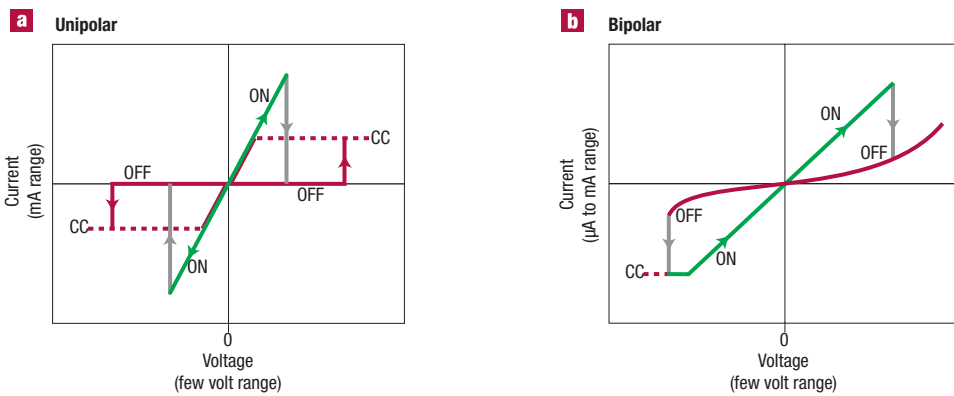


**Figure 1** Classification of the switching characteristics in a voltage sweeping experiment. Depending on the specific system, the curves vary considerably. The purpose of these sketches is to differentiate between the two possible switching directions. Dashed lines indicate that the real voltage at the system will differ from the control voltage because of the compliance current (CC) in action. **a**, Unipolar switching. The set voltage is always higher than the voltage at which reset takes place, and the reset current is always higher than the CC during set operation. **b**, Bipolar switching. The set operation takes place on one polarity of the voltage or current, and the reset operation requires the opposite polarity. In some systems, no CC is used.

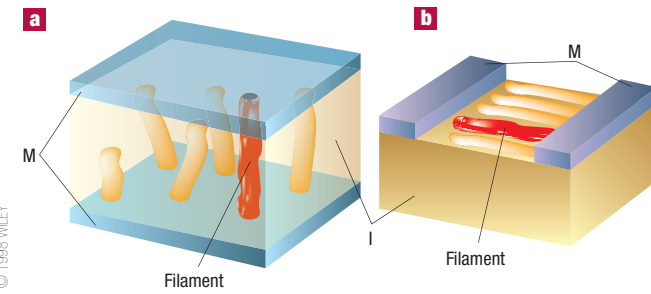


**Figure 2** Sketch of filamentary conduction in MIM structures. Redrawn with modifications from ref. 4. **a**, Vertical stack configuration. **b**, Lateral, planar configuration. The red tube indicates the filament responsible for the ON state.

(Fig. 2). For both cases, in the perpendicular direction (along the path between the electrodes), evidence for interface effects are more frequently described than bulk switching effects.

Conceivable mechanisms for the resistive switching in MIM systems often consist of a combination of physical and/or chemical effects. As a first approach, however, they can be classified according to whether the dominant contribution comes from a thermal effect, an electronic effect, or an ionic effect. Caution must be exercised, because in many reports the switching mechanism has not yet been elucidated or suggestions are based on little experimental and theoretical evidence. Unfortunately, papers often do not report full details of the sample preparation and electrode deposition, the polarity of voltage applied during electroforming and during the first voltage pulse or voltage sweep, the electrode pad-size dependence of the current, the temperature dependence of the electrical response, the yield and the statistics in the cell-to-cell data, or the shift of characteristics on repeated cycling. As a consequence, in many cases we cannot make a comparison of the results and a reasonable assignment of a switching mechanism. Therefore, we attempt a coarse-grained classification of conceivable mechanisms and try to assign selected examples.

A typical resistive switching based on a thermal effect shows a unipolar characteristic. It is initiated by a voltage-induced partial dielectric breakdown in which the material in a discharge filament

is modified by Joule heating. Because of the compliance current, only a weak conductive filament with a controlled resistance is formed. This filament may be composed of the electrode metal transported into the insulator, carbon from residual organics<sup>4</sup> or decomposed insulator material such as sub-oxides<sup>8</sup>. During the reset transition, this conductive filament is again disrupted thermally because of high power density of the order of  $10^{12} \text{ W cm}^{-3}$  generated locally, similar to a traditional household fuse but on the nanoscale. Hence, we refer to this mechanism as the fuse–antifuse type. One candidate out of many is NiO, first reported in the 1960s<sup>9</sup>. Recently, the filamentary nature of the conductive path in the ON state has been confirmed for NiO (ref. 10) and TiO<sub>2</sub> (ref. 11). Cells based on Pt/NiO/Pt thin films have been successfully integrated into CMOS (complementary metal oxide semiconductor) technology to demonstrate non-volatile memory operation<sup>12</sup>. A critical parameter for this unipolar switching effect seems to be the value of the compliance current. In fact, it has recently been demonstrated that a TiO<sub>2</sub> thin film shows bipolar switching, and that this can be changed to unipolar switching characteristics by setting the compliance current to a larger value<sup>13</sup>.

Electronic charge injection and/or charge displacement effects can be considered as another origin of resistive switching. One possibility is the charge-trap model<sup>14</sup>, in which charges are injected by Fowler–Nordheim tunnelling at high electric fields and subsequently trapped at sites such as defects or metal nanoparticles in the insulator. This modifies the electrostatic barrier character of the MIM structure and hence its resistance, resembling the gate-channel resistance in a Flash field-effect transistor (FET). For example, gold nanoclusters incorporated in either polymeric<sup>15,16</sup> or inorganic insulator films<sup>17</sup> can be trapping sites. In a modified model, trapping at interface states is thought to affect the adjacent Schottky barrier at various metal/semiconducting perovskite interfaces<sup>18–20</sup>. A similar mechanism has been reported for ZnSe–Ge heterojunctions<sup>21</sup>.

Another possible model is the insulator–metal transition (IMT), in which electronic charge injection acts like doping to induce an IMT in perovskite-type oxides such as (Pr,Ca)MnO<sub>3</sub> (refs 5,22,23) and SrTiO<sub>3</sub>:Cr (ref. 24). A generic model by Rozenberg *et al.*<sup>25</sup> has recently been extended to bipolar switching<sup>26</sup>.

Finally, a model based on ferroelectricity has been proposed by Esaki<sup>27</sup> and theoretically described by Kohlstedt *et al.*<sup>28,29</sup>. Here, an ultrathin ferroelectric insulator is assumed whose ferroelectric polarization direction influences the tunnelling current through the insulator.

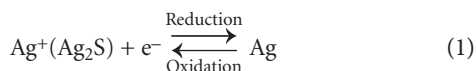
In this review, we will focus on MIM systems in which ionic transport and electrochemical redox reactions provide the essential mechanism for bipolar resistive switching. It is this area in which nanoelectronics<sup>30</sup> becomes intimately connected to nanoionics<sup>31</sup>. One class in this category relies on the sequence of the following processes: the oxidation of an electrochemically active electrode metal such as Ag; the drift of the mobile  $\text{Ag}^+$  cations in the ion-conducting layer; their discharge at the (inert) counterelectrode leading to a growth of Ag dendrites, which form a highly conductive filament in the ON state of the cell<sup>32</sup>. When the polarity of the applied voltage is reversed, an electrochemical dissolution of the conductive bridges takes place, resetting the system into the OFF state. Instead of silver, it is possible to use copper and other metals in the moderate area of the standard electrochemical potential series. A second class in this category operates through the migration of anions, typically oxygen ions, towards the anode (better described by the migration of oxygen vacancies towards the cathode), a subsequent change of the stoichiometry, and a valence change of the cation sublattice associated with a modified electronic conductivity. We will outline the main similarities and differences between the two classes, summarize the current state of knowledge and technology, and sketch future work in this area.

#### REDOX PROCESSES INDUCED BY CATION MIGRATION

Silver growth from heated argentite ( $\alpha\text{-Ag}_2\text{S}$ ) was reported more than 400 years ago<sup>33</sup>. Extensive studies following the first study of electric conduction of  $\text{Ag}_2\text{S}$  by Faraday in the early nineteenth century<sup>34</sup> established the thermodynamical theory of ionic conduction which is a key characteristic of a solid electrolyte. A galvanic cell was used to control stoichiometric deviation of  $\text{Ag}^+$  cations in  $\text{Ag}_2\text{S}$  crystals<sup>35</sup>, and this revealed a mechanism for the silver whisker growth.

By using solid electrolytes in which conduction is due to metal cations, the formation and annihilation of a metal filament in the MIM system can be controlled. To achieve the bipolar switching behaviour, the MIM system consists of an electrode made from an electrochemically active metal, a solid electrolyte as an ion-conducting T layer, and a counter electrode made from an inert metal. Switching behaviour due to silver dendrite formation and annihilation was first reported by Hirose in 1976 using Ag-photodoped amorphous  $\text{As}_2\text{S}_3$  as T of a MIM system with a lateral structure<sup>36</sup>. Kozicki *et al.* succeeded in developing the MIM system in a vertical configuration by using GeSe as the ion conductor and applied this to making non-volatile memory<sup>6</sup>. Recently, resistive switching GeSe structures as small as 20 nm have been fabricated (Fig. 3).

In these systems, metal cations in the ionic conductors migrate towards the cathode made of inert materials and are reduced there. The reduced metal atoms form a metal filament which grows towards the anode to turn on the switch. As the anode is made of electrochemically active material, metal atoms of the anode are oxidized and dissolved into the ionic conductor, maintaining the number of metal cations for continuous electrochemical deposition. In the case of  $\text{Ag}_2\text{S}$ , the following chemical reaction occurs at the anode and the cathode:



On changing the polarity of the bias voltage, metal atoms dissolve at the edge of the metal filament, eventually annihilating the filament so that the switch is turned off. Because the chemical reaction ideally does not cause any damage to the MIM system, the switch may in principle be expected to work indefinitely<sup>6</sup>.

Solid electrolyte can be used as one of the ‘metal’ electrodes of the MIM system. Terabe *et al.* developed this type of MIM switch using an electronic and ionic mixed conductor for one of the electrodes<sup>32</sup>. In this case, a vacuum nano-gap is used as an insulator layer, and a metal

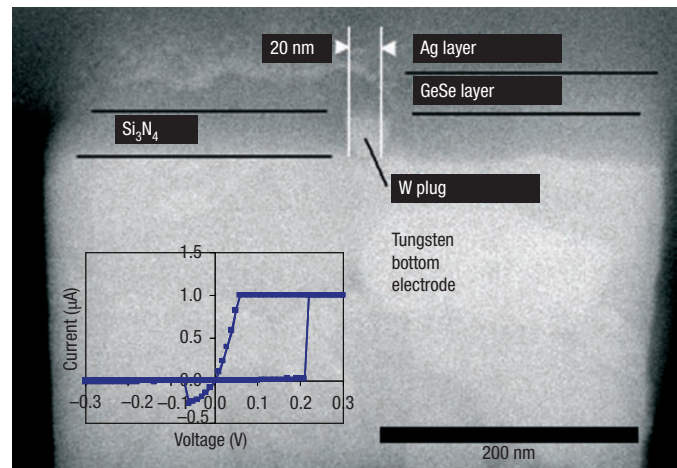


**Figure 3** Cross-section of a vertical type of MIM switch using  $\text{Ag}^+$  conducting solid electrolyte. A silver filament is electrochemically formed in the GeSe layer to turn on the switch. The cross-section is shown for the device for which the inset  $I-V$  curve was recorded. Reprinted with permission from ref. 44.

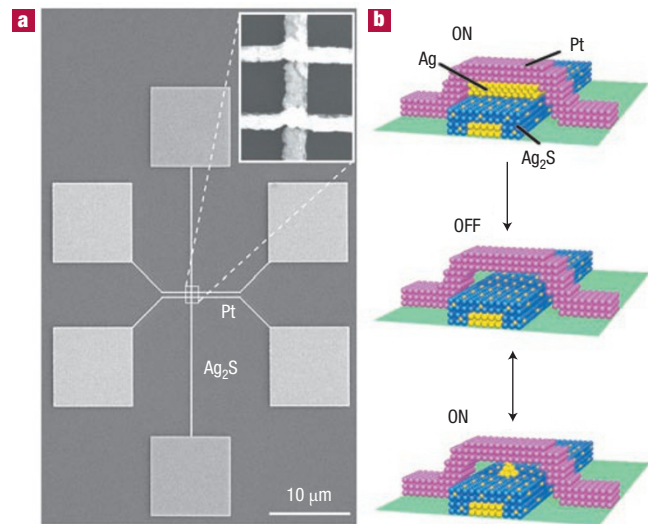


**Figure 4** Scanning electron micrograph of an atomic switch and its operating mechanism<sup>32</sup>. Silver atoms precipitated from the  $\text{Ag}_2\text{S}$  electrode make a bridge in a vacuum gap of 1 nm between the two electrodes. From ref. 32.

filament grows in the gap to bridge the mixed conductor electrode and the counterelectrode (Fig. 4). Because the switching is caused by an electrochemical reaction, increasing a switching bias voltage shortens the switching time exponentially<sup>37</sup>. Reducing the size of a metal filament also produces faster switching.

In both types of MIM system, the switching effect is most easily found for material systems that are cation conductors for the redox active species (such as  $\text{Ag}^+$  in  $\text{Ag}_2\text{S}$ ) or, alternatively, compounds with high solubility of the redox active cation (such as  $\text{Ag}^+$  in  $\text{GeSe}_x$ ). The switches can be operated with smaller bias voltage, such as 0.2 V, which may be preferable for memory devices with low power consumption<sup>6,38</sup>.

Some applications, such as non-volatile switches in reconfigurable large-scale integrated systems (LSIs), require higher threshold bias

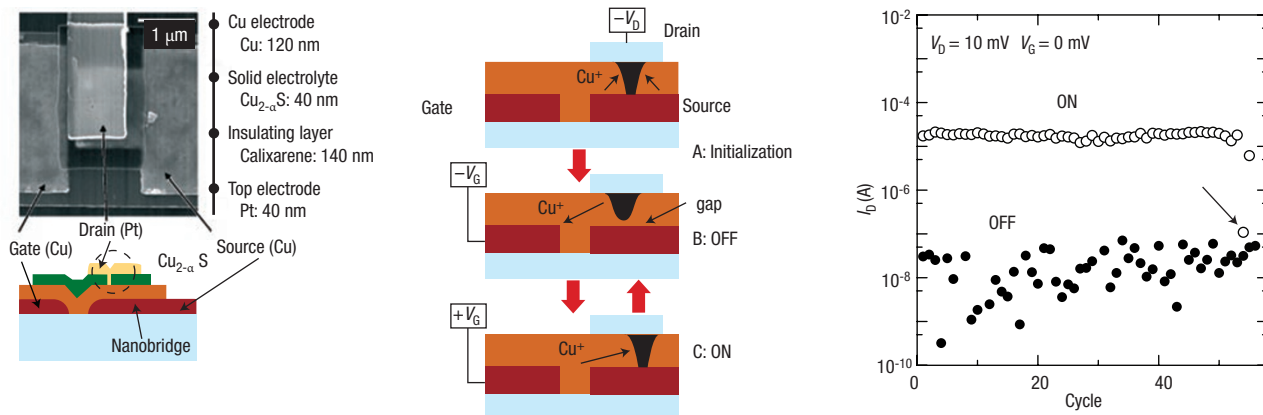


**Figure 5** Three-terminal solid electrolyte switch. Electrochemical reaction for formation and annihilation of a metal filament between the source and the drain electrodes is controlled by the gate voltage. Reprinted with permission from ref. 47.

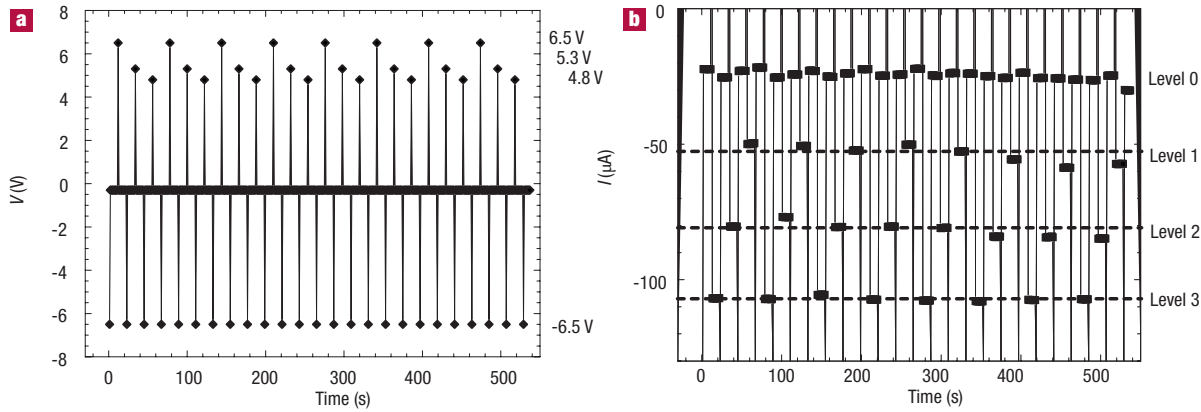


**Figure 6** Multilevel switching in a Cr-doped  $\text{SrZrO}_3$  MIM cell operated at 77 K. **a**, Voltage stimulation. **b**, Current response. Reprinted with permission from ref. 7. By applying voltage pulses of appropriate levels, the system can be set to three different ON state resistances (levels 1 to 3). Together with the OFF state (level 0) this represents a two-bit memory cell.

voltages than that of CMOS devices<sup>38</sup>. Because the switching bias voltage is mainly determined by the activation energy for the chemical reaction and the ionic diffusion constant, the operating bias voltage can be tuned by choice of materials for MIM systems, especially the ion-conducting material. For instance,  $\text{Ta}_2\text{O}_5$  with Cu cations has been reported<sup>39</sup> to have an operating bias voltage of 2 V. Therefore, switches using a variety of solid electrolyte materials such as  $(\text{Zn}, \text{Cd})\text{S}$ ,  $\text{WO}_3$ , and  $\text{SiO}_2$  are being investigated<sup>40–42</sup>. It is interesting to note that systems such as  $\text{Ag}/(\text{Zn}, \text{Cd})\text{S}/\text{Pt}$ , which were initially attributed to a completely different category<sup>43</sup>, are now shown to fall into this cation-migration class<sup>40</sup>. The state of the art with respect to non-volatile memories is demonstrated by  $\text{Ag}/\text{GeSe}_x/\text{W}$  cells integrated into 90-nm CMOS technology<sup>44,45</sup>. In this work, an active matrix concept with one access transistor per switching cell has been used and a prototype integration density of 2 Mbit has been achieved.

Making use of an electrochemical reaction makes it possible to configure three-terminal devices in which switching can be controlled by the gate electrode. Gate-controlled formation and annihilation of a metal filament was first demonstrated by using (liquid) electrolyte<sup>46</sup>, and it has been confirmed with fully solid-state three-terminal devices

(Fig. 5)<sup>47</sup>. Such devices, in which the control line is separated from the conduction line, widen the possibility of practical use of the solid electrolyte switches.

Although the electrochemistry of the cation-migration-based resistive switching cells is reasonably well understood, some questions remain open: for example, the microscopic nature of the cation conduction paths; the impact of thermal effects, details of the electrode reactions in particular for the OFF switching, as well as the interrelationship of the electrolyte nature, the cell geometry and the morphology of the metal dendrites on the nanoscale. In specific systems, such as the  $\text{GeSe}_x$  electrolyte, the role of defects that are also known to affect phase-change alloys has not been clarified yet<sup>48</sup>.

#### REDOX PROCESSES INDUCED BY ANION MIGRATION

In many oxides, in particular in transition metal oxides, oxygen ions defects, typically oxygen vacancies, are much more mobile than cations. If the cathode blocks ion exchange reactions during an electroforming process, an oxygen-deficient region starts to build and to expand towards the anode. Transition metal cations accommodate

this deficiency by trapping electrons emitted from the cathode. In the case of  $\text{TiO}_2$  or titanates, for example, this reduction reaction



is equivalent to filling the Ti 3d band. The reduced valence states of the transition metal cations which are generated by this electrochemical process typically turn the oxide into a metallically conducting phase, such as  $\text{TiO}_{2-n/2}$  for approximately  $n > 1.5$ . This ‘virtual cathode’ moves towards the anode and will finally form a conductive path<sup>49</sup>. At the anode, the oxidation reaction may lead to the evolution of oxygen gas, according to



where  $\text{V}_\text{O}^+$  denotes oxygen vacancies with a double positive charge with respect to the regular lattice and  $\text{O}_\text{O}$  represents an oxygen ion on a regular site according to the Kröger–Vink notation. As an alternative to reaction (3), the anode or the material nearby may be oxidized. The electroforming conditions depend on the MIM system. Macroscopic single crystals typically require some 100 V for several hours, whereas for thin films the first switching cycle at about 1 V may be sufficient. The total charge has been found to control the electroforming<sup>50</sup>. Once the electroforming is completed, the bipolar switching obviously takes place through local redox reactions between the virtual cathode and the anode, by forming or breaking the conductive contact. Depending on the charge transfer during the switching, the resistance of the system can be established at intermediate levels, which might help in creating multibit storage in future memory cells (Fig. 6)<sup>7</sup>.

As in the case of the electrochemical metallization process,  $R_{\text{ON}}$  is usually not pad-size dependent, indicating a filamentary switching in MIM structures, as reported, for example, for nanocrystalline  $\text{Ta}_2\text{O}_5$  and  $\text{Nb}_2\text{O}_5$  thin films<sup>51</sup>,  $\text{VO}_2$  thin films<sup>52</sup>,  $\text{TiO}_2$  thin films<sup>11</sup>, nanoscale confined  $\text{TiO}_2$  (ref. 53) and epitaxial  $\text{SrZrO}_3\text{:Cr}$  thin films<sup>54</sup>. Use of a conductive-tip atomic force microscope (C-AFM) technique has shown the conductive filaments to be identical to dislocations in the case of undoped  $\text{SrTiO}_3$  single crystals and thin films<sup>55</sup>. Figure 7 shows that the conductivity enhancement by several orders of magnitude is confined to a region 1–2 nm wide at the exit of a dislocation. By repeated scanning with a suitably biased AFM tip, the dislocation can be made to switch between an ON and an OFF state. In the ON state, the conductivity shows metallic behaviour, in accordance with first principles calculations<sup>55</sup>. At the surface of ultrathin epitaxial  $\text{SrTiO}_3$  films, entire areas can be reversibly switched between an ON and OFF state by C-AFM (Fig. 8). For these films also, high-resolution studies reveal the filamentary nature of the conductivity and their possible correlation to dislocations<sup>56</sup>. In the case of other materials, such as  $(\text{La},\text{Sr})\text{MnO}_3$  thin films, the conductivity is confined to boundary regions between islands of about 100 nm diameter<sup>57</sup>.

Lateral MIM configurations allow for the observation of filaments along their extension between the electrodes. In undoped  $\text{SrTiO}_3$  single crystals, the formation of conductive filaments within a network of dislocations has been verified by combining electrocoloration studies by optical microscopy with C-AFM scans (Fig. 9)<sup>55</sup>. Infrared thermal microscopy of a Cr-doped  $\text{SrTiO}_3$  single crystal during a current load of 5 mA confirms the confinement of the current path and shows a ‘hot spot’ near the electrode, where the virtual cathode touches the anode (Fig. 10)<sup>58</sup>.

It must be noted that this class of ion-migration-based switching effects is much less well understood than the switching induced by cation migration that was described in the previous section. Open questions remain about the microscopic details of the ion transport, the defect structure and electronic charge transport properties of the

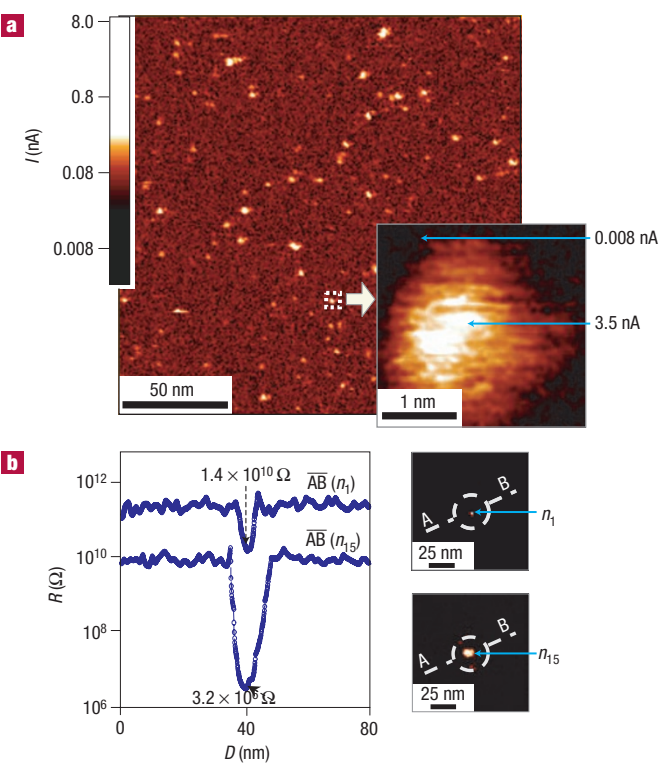
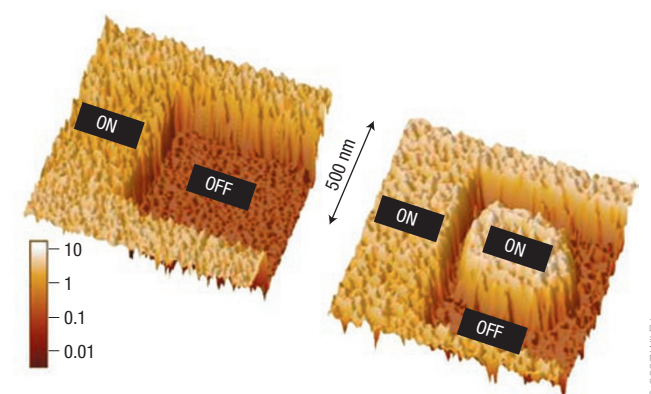


**Figure 7** Conductance of individual dislocations in  $\text{SrTiO}_3$ . **a**, A conductivity map of the surface of an undoped  $\text{SrTiO}_3$  single crystal as recorded by C-AFM after modest thermal reduction. **b**, Line scan across the selected spot ( $D$  denoting the distance along AB) showing the dynamic range of the conductance increase as a result of the application of a negative voltage to the AFM tip. Right: conductivity maps of the selected spot before and after electroformation. From ref. 55.



© 2007 WILEY

**Figure 8** Area-wide switching of an epitaxial 10-nm  $\text{SrTiO}_3$  thin film by C-AFM. The left scan is produced with a tip voltage of  $-6$  V and subsequently with  $+6$  V in the inner area; the right scan is subsequently scanned with  $-6$  V within the inner ON-state area. Reprinted with permission from ref. 56.

conductive channels formed, details of the electrochemical redox reactions involved, and so forth. In several cases, it is not even clear what ions are involved in the process and whether the system falls into the cation- or anion-migration class.

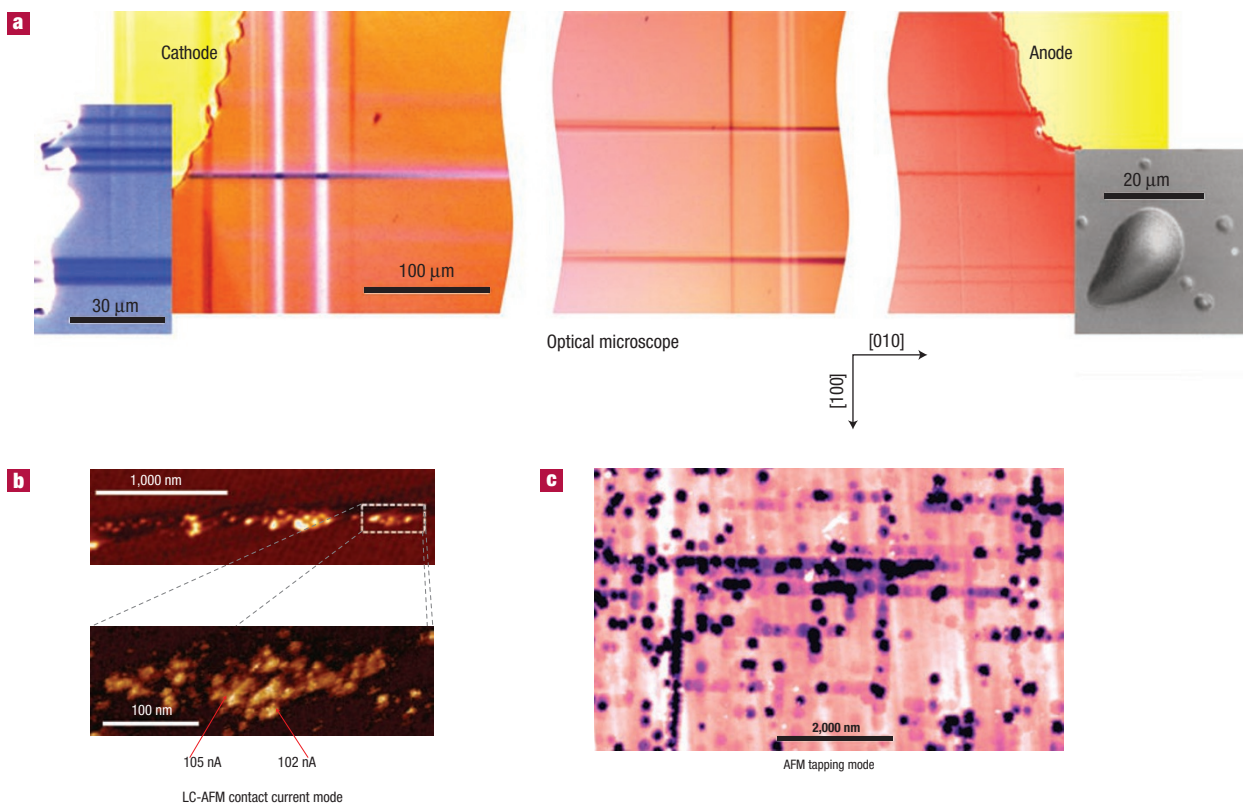


**Figure 9** Filamentary structure induced by electroformation in an undoped SrTiO<sub>3</sub> single crystal. From ref. 55. **a**, Optical micrograph of the filamentary structure created in the skin region of a thermally pre-reduced crystal by electroformation between planar gold electrodes. Segments from left to right: near the cathode, in the central region, and near the anode. Clearly visible is the orthogonal network along the crystallographic [100] direction of the crystal. Insets show the possible fine structure of filaments at the cathode (left) and gas bubble that have developed under the anode metal (right). **b**, High resolution of the scene as recorded by C-AFM at a location between the electrodes, where filaments have terminated at the surface. Measurements support the filamentary character of conductance and the fine structure of the high-conductivity spots. **c**, Etch pits of the same kind of crystal give an example of the distribution of dislocations crossing the surface, highlighting the natural tendency to agglomerate along crystallographic directions.

#### RESISTIVELY SWITCHING SYSTEMS INVOLVING ORGANIC MOLECULES

Resistive switching has been seen in a large variety of MIM systems in which the 'T' layer is represented by organic molecules or polymers of typically 30 nm to >1 μm thickness<sup>59–61</sup>. The characteristics of the organic compounds include redox activity, the formation of a charge-transfer complex, and the formation of donor–acceptor couples. A recent review<sup>62</sup> summarizes the literature comprehensively and classifies the conceivable switching mechanisms, but in many cases the database is too weak to draw definite conclusions. Note that in several studies an aluminium top electrode has been used that is deposited onto the organic layer in an *ex situ* deposition step. Recent control experiments indicate that the organic layer is not always essential for the switching. Instead the switching event seems to take place in a thin Al<sub>2</sub>O<sub>3</sub> layer inevitably formed between the organic layer and the aluminium metal, as found for rose Bengal<sup>63</sup>, for polyethylenedioxythiophene (PEDOT)<sup>64</sup>, and for Cu-tetracyanoquinodimethane (Cu-TCNQ)<sup>65</sup>. In the latter case, a thin aluminium oxide/hydroxide layer was suggested as the conducting layer for copper ions in a cation-migration-based electrochemical switch.

In another class of potential molecular memories, the 'T' layer in a MIM system is a monomolecular film or even a single molecule contacted by a metal tip on the nanoscale. The aim of these molecular electronic studies is to make use of processes such as molecular redox, molecular configuration and conformation changes, or molecular electronic excitations, as well as molecular spin properties that may

affect the electron transfer coefficient<sup>66</sup>. In one of the experiments, however, in which a redox process within a specific catenane molecule was originally attributed to the resistive switching of a monolayer<sup>67</sup>, a control experiment using electronically inactive alkanoic acids revealed a very similar *I*–*V* behaviour<sup>68</sup>, and a conceivable mechanism based on the electrochemistry of the oxide layers formed at the metal electrodes has been suggested<sup>69</sup>.

These examples show that great care must be exercised in attributing mechanistic models to observed switching events and that many critical control experiments are required to obtain an microscopic understanding. Certainly, specific organic molecules have advantageous electronic properties. But the inherent characteristics of these molecules are easily masked by the electrode materials and the experimental boundary conditions. The redox activity of viologen molecules unveiled in an electrochemical *in situ* experiment using scanning tunnelling microscopy (STM)<sup>70,71</sup> and of specific oligophenylene molecules in mechanically controllable break-junction experiments<sup>72</sup> are some of the rare examples in which inherent molecular properties are observed.

#### CHIP ARCHITECTURE, RELIABILITY, SCALING AND OUTLOOK

In a random access memory (RAM) the storage cells are organized in a matrix. Along the rows and columns of the matrix, there are write and read lines, respectively, which are connected to electronic line drives and sense amplifiers in the periphery of the matrix<sup>30</sup>.

Resistive switching storage cells may be organized in a passive cross-bar matrix, just connecting the word and bit lines at each node. The detailed circuit requirements depend on the type (unipolar or bipolar) of switch. Alternatively, in an active matrix, there is a select transistor at each node which decouples the storage cell if it is not addressed. This concept significantly reduces crosstalk and disturb signals in the matrix. Although a passive matrix can, in principle, be fabricated on a  $(4/n)F^2$  scheme per cell (where  $F$  denotes the minimum feature size of the fabrication technology and  $n$  the number of memory layers in a multilayer stack), the cells in an active matrix require somewhat more space, of the order of 4 to  $8F^2$ . Both passive matrices<sup>38,73,74</sup> and active matrices<sup>12,45</sup> have been realized in prototype RRAMs. In passive arrays the storage cells need to incorporate diodes in series with the switchable resistors in order to avoid signal bypasses by cells in the ON state. For oxide-based unipolar cells, a sandwich concept has been proposed to integrate the diode function<sup>75</sup>. In the case of bipolar cells, serial elements with a Zener diode or varistor characteristic are required. In addition, for medium and large passive matrices the interconnect resistances must be taken into account, requiring dedicated reference schemes<sup>76</sup>.

Resistive switching cells offer application opportunities that go beyond mere high-density memory devices. In particular, they can be used as reconfigurable switches in field-programmable gate-array (FPGA) type logic too. About 10 years ago, the Hewlett-Packard research labs developed a prototype computer, called the Teramac, entirely built from conventional, CMOS-based FPGAs, interconnected through several hierarchical levels by a 'fat tree'<sup>77</sup>. They replaced the traditional computer programming based on von Neumann architecture by reconfiguration of the look-up matrices in the FPGAs of the Teramac. The concept proved to be efficient and, as a particular benefit, highly defect-tolerant because during the configuration phase routes could be made around all defects. Defect tolerance is one of the essential demands on any future computer as the defect rate will inherently increase with decreasing feature sizes. The far-reaching idea of the Teramac project has been to replace the complex cells in the conventional FPGAs by nanoscale two-terminal resistive switches. In recent years, considerable progress has been made in resistively switching matrices (described in this review) and in the further elaboration of the architecture concept<sup>78–81</sup>.

Compared with several other emerging memory concepts, the RRAM concept including its different variants is immature. As a consequence, the performance and reliability, and in particular the microscopic mechanism of processes limiting the reliability, have not yet been studied in detail. First results look promising. Switching times of under 10 ns have been reported for individual oxide cells<sup>82</sup>. In the case of cation-migration-induced processes, fatigue of the switching hysteresis of high-density RRAM prototypes did not occur within  $10^6$  write cycles and  $10^{12}$  read cycles<sup>12,83</sup>. A data retention time of over 10 years has been extrapolated, for example, for Ag/GeSe<sub>x</sub> RRAMs<sup>83</sup>. Yet these are just first results. Once we fully understand the particular switching mechanisms, we will need detailed studies of reliability, including a thorough investigation of all conceivable failure mechanisms, and optimization steps based on these.

For the further evolution of nanoelectronics, the question of inherent physical limits to scaling as well as possible technological barriers to scaling is most important. One ultimate limit will be given by the tunnelling distance between neighbouring cells as well as the leakage current from the word and bit line, again potentially dominated by tunnelling<sup>84</sup>. Another limit is obviously set by the lateral extension of the switching area, typically the cross-section of the switching filament as described above. These limits depend on the class of the resistive switching mechanism. The scaling of thermally switching cells will depend on the specific heat capacities and thermal conductivities of the materials involved in the cell, limiting the scaling by the onset of thermal cross-talk as in PCRAMs<sup>48</sup>. Cells based on electrical effects depend on the size of electrostatic barriers controlled

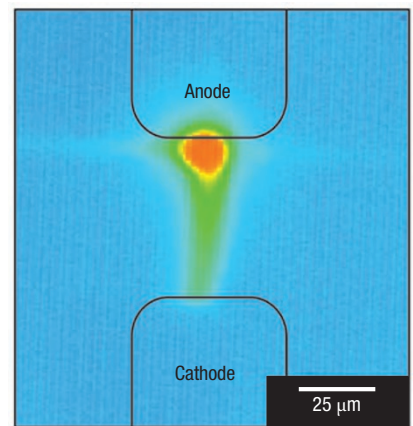


**Figure 10** Infrared thermal micrograph of a planar Cr-doped SrTiO<sub>3</sub> single-crystal cell. The cell has a current of 5 mA at an applied voltage of 30 V. In the colour scale, blue and red represent room temperature and elevated temperature, respectively. From ref. 58.

by the shift of the charges involved<sup>85</sup>. Ionic switching cells may be limited in scaling by the random diffusion of migrating ions involved as well as the metal atoms, in the case of cation-migration-induced redox switching. They may also be limited by poor uniformity due to inherent impurities in the materials. If this is the case, then obviously the downscaling may be limited by the requirements of data retention. Proper selection of materials for their diffusion rates and precisely defined material interfaces on the atomic scale may limit this problem to the point that it falls beyond the ultimate tunnelling limit. In this respect, ion-migration-induced redox-type switching might offer huge potential for future high-density non-volatile memories.

Technologically, the scaling of the RRAMs will be determined by the fabrication of efficient and reliable electrode contacts and interconnects within the matrix. Although great progress has been made in recent years<sup>74,78</sup>, the structures are still far from any tunnelling limit. Another obvious limit to scaling of the chip size will be the size of the periphery circuit and, for active matrices, the size of the access transistors within the matrix. Concepts have been proposed in which the resistive switching cross-bar matrix is slightly rotated against the array of CMOS cells underneath, lifting the alignment constraints considerably<sup>80,86</sup>. This approach can be used to continue the downscaling of the resistive switching cells without having to shrink the access transistors.

Much research effort is still needed to explore the potential of the resistive switching effect in general, and ion-migration-based redox effects in particular, and to exploit this potential to its limits. Questions requiring further attention include a deeper understanding of the microscopic mechanism of the switching, the process and material optimization, the effects limiting the reliability, all aspects of fabrication technology, and the guidelines for scaling.

doi:10.1038/nmat2023

## References

- Hickmott, T. W. Low-frequency negative resistance in thin anodic oxide films. *J. Appl. Phys.* **33**, 2669–2682 (1962).
- Dearnaley, G., Stoneham, A. M. & Morgan, D. V. Electrical phenomena in amorphous oxide films. *Rep. Prog. Phys.* **33**, 1129–1191 (1970).
- Oxley, D. P. Electroforming, switching and memory effects in oxide thin films. *Electrocomponent Sci. Technol. UK* **3**, 217–224 (1977).
- Pagnia, H. & Sotnik, N. Bistable switching in electroformed metal-insulator-metal devices. *Phys. Status Solidi* **108**, 11–65 (1988).
- Asamitsu, A., Tomioka, Y., Kuwahara, H. & Tokura, Y. Current switching of resistive states in magnetoresistive manganites. *Nature* **388**, 50–52 (1997).
- Kozicki, M. N., Yun, M., Hilt, L. & Singh, A. Applications of programmable resistance changes in metal-doped chalcogenides. *Pennington NJ USA: Electrochem. Soc.* 298–309 (1999).

7. Beck, A., Bednorz, J. G., Gerber, C., Rossel, C. & Widmer, D. Reproducible switching effect in thin oxide films for memory applications. *Appl. Phys. Lett.* **77**, 139–141 (2000).
8. Chudnovskii, F. A., Odynets, L. L., Pergament, A. L. & Stefanovich, G. B. Electroforming and switching in oxides of transition metals: the role of metal-insulator transition in the switching mechanism. *J. Solid State Chem.* **122**, 95–99 (1996).
9. Bruyere, J. C. & Chakraverty, B. K. Switching and negative resistance in thin films of nickel oxide. *Appl. Phys. Lett.* **16**, 40–43 (1970).
10. Kim, D. C. *et al.* Electrical observations of filamentary conductances for the resistive memory switching in NiO films. *Appl. Phys. Lett.* **88**, 202102 (2006).
11. Choi, B. J. *et al.* Resistive switching mechanism of TiO<sub>2</sub> thin films grown by atomic-layer deposition. *J. Appl. Phys.* **98**, 033715 (2005).
12. Baek, I. G. *et al.* Highly scalable nonvolatile resistive memory using simple binary oxide driven by asymmetric unipolar voltage pulses. *IEDM Tech. Digest*, 587–590 (2005).
13. Jeong, D. S., Schroeder, H. & Waser, R. Coexistence of bipolar and unipolar resistive switching behaviors. *Electrochim. Solid-State Lett.* **10**, G51–G53 (2007).
14. Simmons, J. G. & Verderber, R. R. New conduction and reversible memory phenomena in thin insulating films. *Proc. R. Soc. Lond. A* **301**, 77–102 (1967).
15. Ouyang, J. Y., Chu, C. W., Szmanda, C. R., Ma, L. P. & Yang, Y. Programmable polymer thin film and non-volatile memory device. *Nature Mater.* **3**, 918–922 (2004).
16. Bozano, L. D. *et al.* Organic materials and thin-film structures for cross-point memory cells based on trapping in metallic nanoparticles. *Adv. Funct. Mater.* **15**, 1933–1939 (2005).
17. Guan, W. *et al.* Fabrication and charging characteristics of MOS capacitor structure with metal nanocrystals embedded in gate oxide. *J. Phys. D* **40**, 2754–2758 (2007).
18. Sawa, A., Fujii, T., Kawasaki, M. & Tokura, Y. Interface resistance switching at a few nanometer thick perovskite manganite active layers. *Appl. Phys. Lett.* **88**, 232112 (2006).
19. Fujii, T. *et al.* Hysteretic current–voltage characteristics and resistance switching at an epitaxial oxide Schottky junction SrRuO<sub>3</sub>/SrTi<sub>0.99</sub>Nb<sub>0.01</sub>O<sub>3</sub>. *Appl. Phys. Lett.* **86**, 012107 (2005).
20. Lee, D. *et al.* in *Proc. Non-Volatile Memory Technology Symposium* (ed. Campbell, K.) 89–93 (IEEE, Piscataway, New Jersey, 2006).
21. Hovel, H. J. & Uggel, J. J. Switching and memory characteristics of ZnSe–Ge heterojunctions. *J. Appl. Phys.* **42**, 5076–5083 (1971).
22. Fors, R., Khartsev, S. I. & Grishin, A. M. Giant resistance switching in metal-insulator-manganite junctions: evidence for Mott transition. *Phys. Rev. B* **71**, 045305 (2005).
23. Kim, D. S., Kim, Y. H., Lee, C. E. & Kim, Y. T. Colossal electroresistance mechanism in a Au/Pr<sub>0.5</sub>Ca<sub>0.5</sub>MnO<sub>x</sub>/Pt sandwich structure: evidence for a Mott transition. *Phys. Rev. B* **74**, 174430 (2006).
24. Meijer, G. I. *et al.* Valence states of Cr and the insulator-to-metal transition in Cr-doped SrTiO<sub>3</sub>. *Phys. Rev. B* **72**, 155102 (2005).
25. Rozenberg, M. J., Inoue, I. H. & Sanchez, M. J. Nonvolatile memory with multilevel switching: a basic model. *Phys. Rev. Lett.* **92**, 178302 (2004).
26. Rozenberg, M. J., Inoue, I. H. & Sanchez, M. J. Strong electron correlation effects in nonvolatile electronic memory devices. *Appl. Phys. Lett.* **88**, 033510 (2006).
27. Esaki, L., Laibowitz, R. B. & Stiles, P. J. Polar Switch. *IBM Tech. Disc. Bull.* **13**, 2161 (1971).
28. Kohlstedt, H., Pertsev, N. A., Contreras, J. R. & Waser, R. Theoretical current–voltage characteristics of ferroelectric tunnel junctions. *Phys. Rev. B* **72**, 125341 (2005).
29. Tsymbal, E. Y. & Kohlstedt, H. Tunneling across a ferroelectric. *Science* **313**, 181–183 (2006).
30. Waser, R. *Nanoelectronics and Information Technology* 2nd edn (Wiley-VCH, Weinheim, 2003).
31. Maier, J. Nanoionics: ion transport and electrochemical storage in confined systems. *Nature Mater.* **4**, 805–818 (2005).
32. Terabe, K., Hasegawa, T., Nakayama, T. & Aono, M. Quantized conductance atomic switch. *Nature* **433**, 47–50 (2005).
33. Ercker, L. *Treatise on Ores and Assaying* (1547) (transl. Sisco, A. G. & Smith, C. S., Univ. Chicago, 1951), p. 177.
34. Faraday, M. *Phil. Trans. R. Soc. Lond.* **123**, 507–522 (1833).
35. Wagner, C. Physical chemistry of ionic crystals involving small concentrations of foreign substances. *J. Phys. Chem.* **57**, 738–742 (1953).
36. Hirose, Y. & Hirose, H. Polarity-dependent memory switching and behaviour of Ag dendrite in Ag-photoinduced amorphous As<sub>2</sub>S<sub>3</sub> films. *J. Appl. Phys.* **47**, 2767–2772 (1976).
37. Tamura, T. *et al.* Switching property of atomic switch controlled by solid electrochemical reaction. *Jpn. J. Appl. Phys.* **45**, L364–L366 (2006).
38. Kaeriyama, S. *et al.* A nonvolatile programmable solid-electrolyte nanometer switch. *IEEE J. Solid-State Circuits USA* **40**, 168–176 (2005).
39. Sakamoto, T. *et al.* A Ta<sub>2</sub>O<sub>5</sub> solid-electrolyte switch with improved reliability. *VLSI Technol. Digest Tech. Pap.* (in the press).
40. Zheng-Wang *et al.* Resistive switching mechanism in Zn<sub>x</sub>Cd<sub>1-x</sub>S nonvolatile memory devices. *IEEE Electron Dev. Lett.* **28**, 14–16 (2007).
41. Kozićki, M. N., Gopalan, C., Balakrishnan, M. & Mitkova, M. A low-power nonvolatile switching element based on copper-tungsten oxide solid electrolyte. *IEEE Trans. Nanotechnol.* **5**, 535–544 (2006).
42. Schindler, C., Puthen Thermadam, S. C., Kozićki, R. & Waser, M. N. Bipolar and unipolar resistive switching in Cu-doped SiO<sub>2</sub>. *IEEE Trans. Electron Dev.* (in the press).
43. van-der-Sluis, P. Non-volatile memory cells based on Zn<sub>x</sub>Cd<sub>1-x</sub>S ferroelectric Schottky diodes. *Appl. Phys. Lett.* **82**, 4089–4091 (2003).
44. Kund, M. *et al.* Conductive bridging RAM (CBRAM): an emerging non-volatile memory technology scalable to sub 20 nm. *IEDM Tech. Digest*, 754–757 (2005).
45. Dietrich, S. *et al.* A nonvolatile 2-Mbit CBRAM memory core featuring advanced read and program control. *IEEE J. Solid-State Circuits* **42**, 839–845 (2007).
46. Xie, F. Q., Nittler, L., Obermaier, C. & Schimmel, T. Gate-controlled atomic quantum switch. *Phys. Rev. Lett.* **93**, 128303 (2004).
47. Banno, N., Sakamoto, T., Hasegawa, T., Terabe, K. & Aono, M. Effect of ion diffusion on switching voltage of solid-electrolyte nanometer switch. *Jpn. J. Appl. Phys.* **45**, 3666–3668 (2006).
48. Wuttig, M. & Yamada, N. Phase change materials for rewriteable data storage. *Nature Mater.* **6**, 824–832 (2007).
49. Baitu, T., Waser, R. & Hardtl, K. H. DC electrical degradation of perovskite-type titanates. III. A model of the mechanism. *J. Am. Ceram. Soc.* **73**, 1663–1673 (1990).
50. Watanabe, Y. *et al.* Current-driven insulator-conductor transition and nonvolatile memory in chromium-doped SrTiO<sub>3</sub> single crystals. *Appl. Phys. Lett.* **78**, 3738–3740 (2001).
51. Pinto, R. Filamentary switching and memory action in thin anodic oxides. *Phys. Lett. A* **35**, 155–156 (1971).
52. Beaulieu, R. P., Sulway, D. V. & Cox, C. D. The detection of current filaments in VO<sub>x</sub> thin-film switches using the scanning electron microscope. *Solid-State Electron.* **3**, 428–429 (1973).
53. Ogimoto, Y., Tamia, Y., Kawasaki, M. & Tokura, Y. Resistance switching memory device with a nanoscale confined current path. *Appl. Phys. Lett.* **90**, 143515 (2007).
54. Rossel, C., Meijer, G. I., Bremaud, D. & Widmer, D. Electrical current distribution across a metal-insulator-metal structure during bistable switching. *J. Appl. Phys.* **90**, 2892–2898 (2001).
55. Szot, K., Speier, W., Bihlmayer, G. & Waser, R. Switching the electrical resistance of individual dislocations in single-crystalline SrTiO<sub>3</sub>. *Nature Mater.* **5**, 312–320 (2006).
56. Szot, K., Dittmann, R., Speier, W. & Waser, R. Nanoscale resistive switching. *Phys. Status Solidi 1*, R86–R88 (2007).
57. Chen, X., Wu, N., Strozier, J. & Ignatiev, A. Spatially extended nature of resistive switching in perovskite oxide thin films. *Appl. Phys. Lett.* **89**, 063507 (2006).
58. Janousch, M. *et al.* Role of oxygen vacancies in Cr-doped SrTiO<sub>3</sub> for resistance-change memory. *Adv. Mater.* **19**, 2232–2235 (2007).
59. Pender, L. F. & Fleming, R. J. Memory switching in glow discharge polymerized thin films. *J. Appl. Phys.* **46**, 3426–3431 (1975).
60. Potember, R. S., Poehler, T. O. & Cowan, D. O. Electrical switching and memory phenomena in Cu-TCNQ thin films. *Appl. Phys. Lett.* **34**, 405–407 (1979).
61. Bandyopadhyay, A. & Pal, A. J. Large conductance switching and memory effects in organic molecules for data-storage applications. *Appl. Phys. Lett.* **82**, 1215–1217 (2003).
62. Scott, J. C. & Bozano, L. D. Nonvolatile memory elements based on organic materials. *Adv. Mater.* **19**, 1452–1463 (2007).
63. Karthauser, S. *et al.* Resistive switching of rose bengal devices: a molecular effect? *J. Appl. Phys.* **100**, 094504 (2006).
64. Colle, M., Buchel, M. & de-Leeuw, D. M. Switching and filamentary conduction in non-volatile organic memories. *Org. Electron.* **7**, 305–312 (2006).
65. Kever, T., Boettger, U., Schindler, Ch. & Waser, R. On the origin of bistable resistive switching in Cu:TCNQ. *Appl. Phys. Lett.* **91**, 083506 (2007).
66. Feringa, B. L. *Molecular Switches* (Wiley-VCH, Weinheim, 2001).
67. Collier, C. P. *et al.* A [2]catenane-based solid state electronically reconfigurable switch. *Science* **289**, 1172–1175 (2000).
68. Stewart, D. R. *et al.* Molecule-independent electrical switching in Pt/organic monolayer/Ti devices. *Nano Lett.* **4**, 133–136 (2004).
69. Blackstock, J. J. *et al.* Internal structure of a molecular junction device: chemical reduction of PtO<sub>2</sub> by Ti. *J. Phys. Chem. C* **111**, 16–20 (2007).
70. Li, Z. *et al.* Two-dimensional assembly and local redox-activity of molecular hybrid structures in an electrochemical environment. *Faraday Disc.* **131**, 121–143 (2005).
71. Li, Z., Pobelov, I., Han, B., Wandlowski, T., Blaszczyk, A. & Mayor, M. Conductance of redox-active single molecular junctions: an electrochemical approach. *Nanotechnology* **18**, 1–8 (2007).
72. Lörtscher, E., Ciszek, J. W., Tour, J. & Riel, H. Reversible and controllable switching of a single-molecule junction. *Small* **2**, 973–977 (2006).
73. Wu, W. *et al.* One-kilobit cross-bar molecular memory circuits at 30-nm half-pitch fabricated by nanoimprint lithography. *Appl. Phys. A* **80**, 1173–1178 (2005).
74. Green, J. E. *et al.* A 160-kilobit molecular electronic memory patterned at 10<sup>11</sup> bits per square centimetre. *Nature* **445**, 14–17 (2007).
75. Lee, M. J. *et al.* A low-temperature grown oxide diode as a new switch element for high-density, nonvolatile memories. *Adv. Mater.* **19**, 73–76 (2007).
76. Mustafa, J. & Waser, R. A novel reference scheme for reading passive resistive crossbar memories. *IEEE Trans. Nanotechnol.* **5**, 687–691 (2006).
77. Heath, J. R., Ruekes, P. J., Snider, G. S. & Williams, R. S. A defect-tolerant computer architecture: opportunities for nanotechnology. *Science* **280**, 1716–1721 (1998).
78. Snider, G., Ruekes, P., Hogg, T. & Williams, R. S. Nanoelectronic architectures. *Appl. Phys. A* **80**, 1183–1195 (2005).
79. DeHon, A., Randy Huang, & Wawrzynek, J. Stochastic spatial routing for reconfigurable networks. *Microprocessors Microsyst.* **30**, 301–318 (2006).
80. Likharev, K. K. & Strukov, D. B. in *Introducing Molecular Electronics. Lecture Notes in Physics Vol. 680* (eds Cuniberti, G., Richter, K. & Fagas, G.) 447–477 (Springer, Berlin, 2006).
81. Lu, W. & Lieber, C. M. Nanoelectronics from the bottom up. *Nature Mater.* **6**, 841–850 (2006).
82. Ignatiev, A. *et al.* Resistance switching in perovskite thin films. *Phys. Stat. Sol. B* **243**, 2089–2097 (2006).
83. Honigschmid, H. *et al.* A non-volatile 2Mbit CBRAM memory core featuring advanced read and program control. *VLSI Circuits Symp. Tech. Digest*, 110–11 (2006).
84. Zhirnov, V. V., Cavin-R-K-III, Hutchby, J. A. & Bourianoff, G. I. Limits to binary logic switch scaling—a gedanken model. *Proc. IEEE USA* **91**, 1934–1939 (2003).
85. Cavin, R. K., Zhirnov, V. V., Herr, D. J. C., Alba Avila, & Hutchby, J. Research directions and challenges in nanoelectronics. *J. Nanoparticle Res.* **8**, 841–858 (2006).
86. Snider, G. S. & Williams, R. S. Nano/CMOS architectures using a field-programmable nanowire interconnect. *Nanotechnology* **18**, 1–11 (2007).

### Acknowledgements

We thank J. G. Bednorz (IBM Research, Zurich), U-In Chung, I. G. Baek and S. O. Park (Samsung Electronics), Y. Zhang (Intel, Santa Clara), R. Bruchhaus (Qimonda, Munich), V. Zhirnov (SRC), and K. Szot and R. Dittmann (Research Center Jülich) for valuable comments. Correspondence and requests for materials should be addressed to R.W.